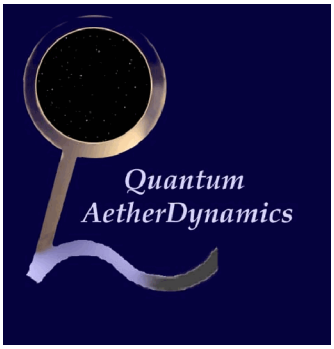

Quantum AetherDynamics Institute (QADI)

Electron EDM in QMU: CP-odd Square-Charge Dipole from Aether-Unit Holonomy

David W. Thomson III
Quantum AetherDynamics Institute (QADI), Alma, Illinois, USA
ORCID: 0000-0002-5830-5427

Version 1.0 – February 17, 2026

This article is published by the Quantum AetherDynamics Institute (QADI).

It develops the Aether Physics Model (APM)

Abstract

In QMU, charge is a square-charge primitive and electrostatic potential is reciprocal capacitance. Therefore an electron "EDM" is not naturally a linear-charge dipole, but a CP-odd *square-charge first moment* with unit ${e_{\mathrm{emax}}}^2 \cdot \lambda_C$ in the distributed-charge basis. We define the observable $\mathbf{D}_{e^2} = \int \rho_{e^2}(\mathbf{r})\,\mathbf{r}\,d^3r$, derive the ledger-closed coupling $\Delta U = -\mathbf{D}_{e^2} \cdot \nabla\Phi_Q$ with $\Phi_Q := 1/C$, and parameterize $\mathbf{D}_{e^2}$ by a dimensionless CP-holonomy invariant $\Delta_{\mathrm{CP}} = (2\pi)^{-1} \oint \delta\omega_{\mathrm{CP}}$. We then commit to a minimal electron domain taxonomy and show how CP-odd holonomy is either forced to cancel (exact geometric neutrality) or quantized by a topological obstruction index. This reframes "probabilistic" EDM constraints as constraints on admissible microstate classes and their packing-weighted populations.

Keywords: QMU; APM; EDM; distributed square-charge; reciprocal capacitance; CP-odd holonomy; domain packing; obstruction index; metrology; ledger closure

1 Introduction

Institutional attribution follows the QADI citation guide Quantum AetherDynamics Institute (QADI) [2025]. EDM searches are a precision route to constraining CP-violating physics and its effective operators across scales; see, e.g., the standard reviews Chupp et al. [2019], Pospelov and Ritz [2005]. A central result of the charge conversion factor (CCF) program Thomson [2025a] is that several legacy interpretations must be rewritten in QMU. For EDM physics, the two decisive rewrites are: (i) electrostatic potential is reciprocal capacitance, $\Phi_Q := 1/C$; (ii) the primitive charge dimension is square-charge (distributed charge in the magnetic basis is ${e_{\mathrm{emax}}}^2$).

Legacy EDM narratives attach a point-parameter d_e to a pointlike electron and couple it to an "electric field." In QMU, the primitive observable is a geometric moment of a distributed square-charge density and its coupling is to a geometric gradient of reciprocal capacitance. This paper formalizes that reframing and places the EDM observable inside an Aether-unit holonomy hierarchy that can be extended upward to macro matter via packing statistics.

2 Ledger Closure Check

$$A_u\,\mathrm{curl} = {F_q}^2\,{\lambda_C}^2. \tag{1}$$

3 QMU potential and its gradient

Define QMU potential as

$$\Phi_Q := \frac{1}{C}. \tag{2}$$

The electrostatic driver is the reciprocal-capacitance gradient

$$\mathbf{G} := \nabla\Phi_Q. \tag{3}$$

In the charge-squared ledger, contracting $\mathbf{G}$ (inverse-area character) with a square-charge dipole (square-charge times length) produces the native Coulomb-energy scaling $\sim$ (square-charge)/length.

4 Square-charge EDM observable

4.1 Distributed square-charge density and first moment

Let $\rho_{e^2}(\mathbf{r})$ be the signed distributed square-charge density of the electron in the magnetic basis. The square-charge dipole vector is the first moment

$$\mathbf{D}_{e^2} := \int \rho_{e^2}(\mathbf{r})\, \mathbf{r}\, d^3r. \tag{4}$$

The unit of $\mathbf{D}_{e^2}$ is ${e_{\text{emax}}}^2 \cdot \lambda_C$. By construction, $\mathbf{D}_{e^2}$ is a polar vector (odd under spatial inversion). A measurable electron EDM corresponds to the existence of a *spin-aligned* polar vector that is simultaneously CP-odd.

4.2 Ledger-closed interaction energy

The QMU interaction energy between a square-charge dipole and external electrostatic structure is

$$\Delta U = -\,\mathbf{D}_{e^2} \cdot \mathbf{G} = -\,\mathbf{D}_{e^2} \cdot \nabla\Phi_Q. \tag{5}$$

Equation (5) is the QMU replacement for the legacy coupling $-\mathbf{d} \cdot \mathbf{E}$. It is not a relabeling: it changes the *driver* from $\mathbf{E}$ to $\nabla\Phi_Q$, consistent with the APM/QMU reinterpretation of potential and capacitance.

5 Why the EDM is not a point-parameter in QMU

In a point-particle narrative the EDM is an intrinsic scalar coefficient attached to a pointlike electron. In QMU this is structurally unnatural because: (1) the primitive charge dimension is square-charge, and (2) the natural EDM observable is a geometric moment (4) of a distributed density. A delta-supported "point" cannot carry a well-defined first moment without introducing an unphysical regulator or hidden internal coordinates. In APM, the required internal coordinates are supplied by the electron's Aether-unit geometry and its 5D-to-4D holonomy projection. Thus the EDM problem becomes: determine whether the Aether packing admits a CP-odd first moment of ρ_{e^2}, and if so, quantify it.

6 Holonomy origin in APM

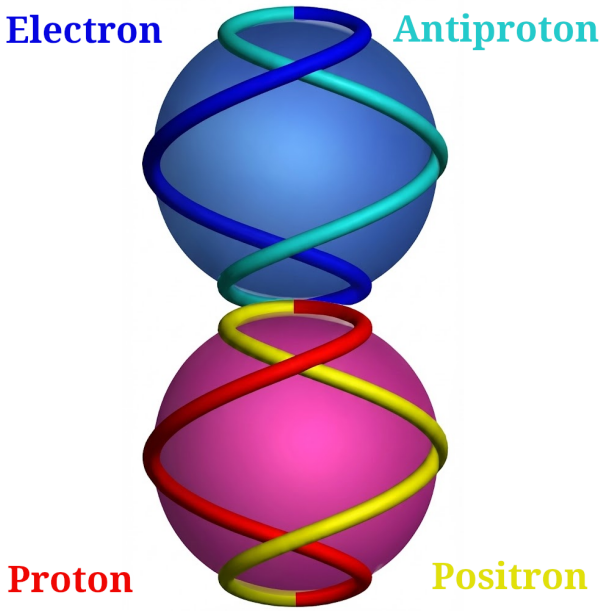

Figure 1: Aether Unit two-sphere geometry with chronovibrational loxodromes. The negative (blue) sphere hosts the negatively charged pair: electron (blue) and antiproton (cyan). The positive (pink/magenta) sphere hosts the positively charged pair: proton (red) and positron (yellow). Forward time expands outward from the Singularity across both spheres toward their antipodes; backward time collapses from the antipodes back to the Singularity. The 5D action closes over the full cycle, while 4D observation samples only the forward-time leg, appearing as holonomy.

6.1 Electrostatic sheet polarity and magnetic dipole structure

The two spheres define the electrostatic polarity dipole of the Aether unit. Electron and antiproton share the negative sheet; proton and positron share the positive sheet. Thus electrostatic charge is not a point-monopole property of an isolated particle: it is inherent to the Aether unit's two-sheet polarity. By contrast, the magnetic square-charge structure is inherent to each of the four spin positions (electron, proton, positron, antiproton) and is intrinsically dipolar; it is not representable as a magnetic monopole.

6.2 Two-sphere chronovibration and half-spin

The Aether unit is a coupled *double-sphere* geometry: two spatial $\mathbb{S}^2$ sheets joined by the Singularity and paired by antipodal correspondence. Forward time begins at the Singularity and propagates *simultaneously over both spheres* toward their antipodes, forming an outward-expanding double-sphere. Backward time begins at the antipodes and propagates back toward the Singularity, forming a collapsing double-sphere. In this way both spheres remain present to the physical Universe during the forward-time expansion, supporting the coexistence of the four stable subatomic particle species (electron, proton, positron, antiproton) as distinct Aether-packings on the two sheets and their

charge-basis conjugates.

A subatomic particle is supported on only one of the two spatial sheets as a *4D-visible* object, but its full 5D action includes a chronovibrational out-and-back cycle. If any evolution occurs purely on the backward-time leg, it is part of the 5D closure yet is not directly accessible to 4D measurement; this is the origin of the apparent "weirdness" of quantum behavior: observed 4D histories are subsets of the full 5D chronovibrational action.

We denote the two spatial sheets by $\mathbb{S}^2_{(1)}$ and $\mathbb{S}^2_{(2)}$. For a given particle species, let $\mathbb{S}^2_{\mathrm{p}} \in \{\mathbb{S}^2_{(1)}, \mathbb{S}^2_{(2)}\}$ denote the sheet on which its *forward-time* transport is supported. Let $\gamma_+ \subset \mathbb{S}^2_{\mathrm{p}}$ be the forward-time (outgoing) loxodromic transport path from the Singularity toward the antipode, and let $\gamma_- \subset \mathbb{S}^2_{\mathrm{p}}$ be the backward-time (return) continuation from the antipode back toward the Singularity under chronovibration. The full chronovibrational cycle is the closed 5D ledger path

$$\Gamma := \gamma_+ \cup \gamma_-. \tag{6}$$

The *half-spin* nature follows because subatomic particles are observed only on the forward-time leg γ_+ as "physical time"; the complementary γ_- leg contributes to 5D closure but is not directly accessible to 4D measurements. Holonomy arises because the 4D projected ledger is evaluated on γ_+ rather than on the full 5D-closed cycle Γ.

6.3 Connection one-forms and the defect form

Let ω_5 denote the intrinsic 5D connection one-form governing transport on the Aether-unit geometry along the electron chronovibrational path γ_+, and let ω_4 be its induced 4D projected connection. Define the raw defect one-form on the path by

$$\delta\omega := \gamma_+^* \omega_5 - \gamma_+^* \omega_4. \tag{7}$$

5D closure vs 4D holonomy. On the full chronovibrational cycle Γ the 5D ledger closure is evaluated, and the corresponding integrated defect vanishes (or is an integer multiple of 2π) by construction:

$$\oint_\Gamma \delta\omega \;=\; 0 \pmod{2\pi}. \tag{8}$$

The observable holonomy relevant to subatomic measurements is the forward-time restriction on γ_+, which need not vanish:

$$\delta_H := \frac{1}{2\pi} \oint_{\gamma_+} \delta\omega. \tag{9}$$

This is the precise sense in which the ledger closes in 5D while remaining nontrivial in 4D.

Introduce the CP transformation $\mathcal{CP}$ on the path data and define the CP-odd projected defect form

$$\delta\omega_{\mathrm{CP}} := \frac{1}{2}\Big(\delta\omega - (\mathcal{CP})^* \delta\omega\Big). \tag{10}$$

By construction, $(\mathcal{CP})^* \delta\omega_{\mathrm{CP}} = -\delta\omega_{\mathrm{CP}}$.

6.4 Dimensionless CP-holonomy invariant

Define the dimensionless CP-holonomy invariant

$$\Delta_{\mathrm{CP}} := \frac{1}{2\pi} \oint_{\gamma_+} \delta\omega_{\mathrm{CP}}. \tag{11}$$

If the electron packing admits no intrinsic chirality in the 5D-to-4D projection, then $\delta\omega_{\mathrm{CP}}$ is exact or cancels under domain pairing and $\Delta_{\mathrm{CP}} = 0$. Otherwise $\Delta_{\mathrm{CP}} \neq 0$ quantifies CP-odd holonomy leakage.

6.5 Square-charge dipole magnitude from holonomy

We adopt the minimal ledger-closed mapping from a dimensionless holonomy invariant to a square-charge dipole:

$$\mathbf{D}_{e^2} = {e_{\mathrm{emax}}}^2 \, \lambda_C \, \Delta_{\mathrm{CP}} \, \hat{\mathbf{s}}. \tag{12}$$

Substituting (12) into (5) yields

$$\Delta U = - {e_{\mathrm{emax}}}^2 \, \lambda_C \, \Delta_{\mathrm{CP}} \, (\hat{\mathbf{s}} \cdot \nabla \Phi_Q). \tag{13}$$

7 Ensemble interpretation and macro-matter bridge

A "probabilistic" EDM constraint is naturally reinterpreted in APM/QMU as a constraint on an *ensemble* of admissible electron domain microstates prepared by external structure, consistent with the general EDM interpretation literature Chupp et al. [2019]. Let $\mathcal{S}$ be the set of admissible microstates s (domain patterns, boundary slips, handedness assignments) with packing weights $w(s)$ satisfying $\sum_{s\in\mathcal{S}} w(s) = 1$. Then

$$\langle \Delta_{\mathrm{CP}} \rangle = \sum_{s\in\mathcal{S}} w(s) \, \Delta_{\mathrm{CP}}(s), \qquad \langle \mathbf{D}_{e^2} \rangle = {e_{\mathrm{emax}}}^2 \, \lambda_C \, \langle \Delta_{\mathrm{CP}} \rangle \, \hat{\mathbf{s}}. \tag{14}$$

In macro matter, constitutive behavior corresponds to coarse-grained summaries of which microstates are admissible and how packing biases their weights $w(s)$. Thus EDM bounds constrain either (i) the admissible CP-odd microstate classes (geometry/topology) or (ii) the degree to which external packing can bias chirality-sector populations (statistics), without requiring intrinsic randomness at the primitive level.

8 Domain taxonomy, quantization, and obstruction index

8.1 Minimal electron domain model

We commit to a minimal octant-domain decomposition of the electron packing on the Aether-unit geometry: $N = 8$ domains, paired antipodally.

No cube. The term "octant" here is a spherical-domain taxonomy on $\mathbb{S}^2_{\mathrm{p}}$, not a cube in physical space. Concretely, in an $\mathbb{R}^3$ embedding of $\mathbb{S}^2_{\mathrm{p}}$ the seams are the great-circle intersections of $\mathbb{S}^2_{\mathrm{p}}$ with

the three coordinate planes $x = 0$, $y = 0$, $z = 0$. These three great circles partition $\mathbb{S}^2_{\mathrm{p}}$ into eight connected regions (four in each hemisphere). The seams are great-circle arcs, and the loxodrome γ_+ crosses these seams in a definite ordered sequence, forming the loxodromic seam loop used in §9.3.

Under $\mathcal{CP}$, antipodal pairing reverses handedness, giving the pairing rule for CP-odd boundary slips

$$\Delta\varphi_{\bar{i}}^{(\mathrm{CP})} = -\,\Delta\varphi_i^{(\mathrm{CP})}. \tag{15}$$

If all boundaries pair, the CP-odd jump sum cancels and the jump sector is neutral.

8.2 Quantized boundary jump spectrum and α^p suppression

Let the fundamental boundary increment be $2\pi/N = \pi/4$. We write CP-odd boundary slips as

$$\Delta\varphi_i^{(\mathrm{CP})} = \sigma_i \frac{\pi}{4}\,\alpha^p, \qquad \sigma_i \in \mathbb{Z}, \quad p \geq 1. \tag{16}$$

The exponent p is *not* fitted: it is the minimal order at which the explicit 5D-to-4D connection admits a CP-odd defect (derived in §9). The α factor appears because CP-odd leakage must involve a basis-mixing channel controlled by the charge conversion structure (CCF) rather than a pure α^0 geometric term; compare the role of operator mixing and loop suppression in standard EDM analyses Pospelov and Ritz [2005], Chupp et al. [2019].

8.3 Topological obstruction index

Define the obstruction index $\tau_{\mathrm{CP}} \in \mathbb{Z}$ to be the net unpaired CP-odd defect content around the closed electron path after antipodal cancellations. Then the discrete spectrum of admissible CP invariants takes the form

$$\Delta_{\mathrm{CP}} = \alpha^p \frac{\tau_{\mathrm{CP}}}{8} \qquad (\tau_{\mathrm{CP}} \in \mathbb{Z}). \tag{17}$$

Equation (17) encodes the central geometric fork: *either* $\tau_{\mathrm{CP}} \equiv 0$ for the electron (exact geometric neutrality), *or* a nonzero obstruction class exists and the EDM is quantized and α-suppressed.

9 Explicit 5D→4D connection ansatz and CP-odd extraction

This section provides the next-step ansatz needed to pin the leading order p in (16) and identify admissible obstruction candidates τ_{CP}.

9.1 Aether-unit transport decomposition

Along the electron path γ_+, decompose the pulled-back connections into CP-even (spin) and CP-odd (chiral) sectors:

$$\gamma_+^*\omega_5 = \omega^{(0)} + \alpha\,\omega_\chi^{(1)} + \alpha^2\,\omega_\chi^{(2)} + \cdots, \qquad \gamma_+^*\omega_4 = \omega^{(0)} + \alpha\,\Pi\omega_\chi^{(1)} + \alpha^2\,\Pi\omega_\chi^{(2)} + \cdots. \tag{18}$$

Here: (i) $\omega^{(0)}$ is the CP-even baseline that projects identically (Dirac-like spin transport); (ii) $\omega_\chi^{(k)}$ are chiral correction one-forms generated by the 5D-to-4D holonomy map; (iii) Π is the 4D projection operator, which may annihilate (or partially annihilate) chiral components.

Under $\mathcal{CP}$, the chiral sector flips sign while $\omega^{(0)}$ is invariant:

$$(\mathcal{CP})^*\omega^{(0)} = \omega^{(0)}, \qquad (\mathcal{CP})^*\omega_\chi^{(k)} = -\,\omega_\chi^{(k)}. \tag{19}$$

9.2 Defect form and leading order

Using (7) and (18), the raw defect is

$$\delta\omega = \alpha\,(I-\Pi)\omega_\chi^{(1)} + \alpha^2\,(I-\Pi)\omega_\chi^{(2)} + \cdots. \tag{20}$$

Applying the CP-odd projector (10) and the sign rule (19) yields

$$\delta\omega_{\mathrm{CP}} = \alpha\,(I-\Pi)\omega_\chi^{(1)} + \alpha^2\,(I-\Pi)\omega_\chi^{(2)} + \cdots. \tag{21}$$

Therefore the minimal admissible order is

$$p = 1 \quad \text{unless symmetry forces } \oint (I-\Pi)\omega_\chi^{(1)} = 0. \tag{22}$$

If the α term integrates to zero by domain pairing or exactness, then the leading order is pushed to $p \geq 2$. This provides a concrete target for the next derivation step: compute $\omega_\chi^{(1)}$ from the explicit holonomy map and test whether its projected defect is exact on each domain.

9.3 Bulk–seam reduction on an octant domain cover and the computable rule for p

Fix an octant domain cover $\{\mathcal{D}_i\}_{i=1}^8$ of the forward-time sheet $\mathbb{S}^2_{\mathrm{p}}$ supporting γ_+, with antipodal pairing $i \leftrightarrow \bar{i}$. Let $\Sigma_i := \gamma_+ \cap \mathcal{D}_i$ denote the segments of the forward path contained in each domain, and let $\mathcal{E}$ denote the set of oriented seams (domain boundaries) crossed by γ_+. We assume the leading CP-odd defect is *locally exact* on each domain at order α^k, i.e.

$$(I-\Pi)\omega_\chi^{(k)}\big|_{\mathcal{D}_i} = d\psi_i^{(k)}, \qquad i = 1,\ldots,8, \tag{23}$$

for domain potentials $\psi_i^{(k)}$ that may fail to agree across seams.

For an oriented seam crossing $e = (i \to j) \in \mathcal{E}$, define the CP-odd stitching jump at order α^k by

$$\Delta\varphi_{ij}^{(\mathrm{CP},k)} \;:=\; \psi_j^{(k)}\big|_e \;-\; \psi_i^{(k)}\big|_e. \tag{24}$$

Antipodal CP pairing enforces the sign rule

$$\Delta\varphi_{\bar{i}\bar{j}}^{(\mathrm{CP},k)} = -\,\Delta\varphi_{ij}^{(\mathrm{CP},k)}. \tag{25}$$

Along the forward leg, the CP-odd holonomy invariant reduces to a seam sum once bulk exactness is imposed:

$$\Delta_{\mathrm{CP}} = \frac{1}{2\pi}\oint_{\gamma_+}\delta\omega_{\mathrm{CP}} = \sum_{k\geq 1}\alpha^k\,\Delta_{\mathrm{CP}}^{(k)}, \qquad \Delta_{\mathrm{CP}}^{(k)} = \frac{1}{2\pi}\sum_{(i\to j)\in\mathcal{E}(\gamma_+)}\Delta\varphi_{ij}^{(\mathrm{CP},k)}. \tag{26}$$

Thus p is *not* a fitted exponent: it is the smallest order at which the seam cocycle is nontrivial on the seam sequence traced by γ_+:

$$p \;:=\; \min\Big\{k \geq 1 : \sum_{(i\to j)\in\mathcal{E}(\gamma_+)} \Delta\varphi_{ij}^{(\mathrm{CP},k)} \neq 0\Big\}. \tag{27}$$

For the octant increment $2\pi/N = \pi/4$, we encode the discrete spectrum of admissible seam jumps by

$$\Delta\varphi_{ij}^{(\mathrm{CP},p)} = m_{ij}\,\frac{\pi}{4}, \qquad m_{ij} \in \mathbb{Z}, \tag{28}$$

so that the forward-leg invariant at leading order takes the integer form

$$\Delta_{\mathrm{CP}} = \alpha^p\,\frac{\tau_{\mathrm{CP}}}{8}, \qquad \tau_{\mathrm{CP}} := \sum_{(i\to j)\in\mathcal{E}(\gamma_+)} m_{ij} \in \mathbb{Z}, \tag{29}$$

which is the seam-cocycle obstruction index induced by the loxodromic seam sequence on the electron sheet.

9.4 Milestone M1: compute $\omega_\chi^{(1)}$ on the loxodromic seam loop

The loxodromic seam loop fixes a concrete ordered set of seam crossings $\mathcal{E}(\gamma_+)$. Milestone M1 is the explicit computation of the leading CP-odd connection $\omega_\chi^{(1)}$ and its seam jumps $\Delta\varphi_{ij}^{(\mathrm{CP},1)}$ along that ordered seam sequence.

(i) Octant seams on $\mathbb{S}^2_{\mathrm{p}}$ and the loxodrome crossing set

Work on the forward-time electron sheet $\mathbb{S}^2_{\mathrm{p}} \cong \mathbb{S}^2$ with spherical coordinates (θ, ϕ) and metric $ds^2 = d\theta^2 + \sin^2\theta\, d\phi^2$. The octant taxonomy is induced by three great circles:

$$\text{(seams)} \qquad \phi = 0,\ \frac{\pi}{2},\ \pi,\ \frac{3\pi}{2}, \qquad \theta = \frac{\pi}{2}. \tag{30}$$

These seams partition $\mathbb{S}^2_{\mathrm{p}}$ into eight connected domains $\{\mathcal{D}_i\}_{i=1}^8$ (four longitude wedges in each of the two hemispheres). No cube is involved; the seams are great-circle arcs.

A loxodrome on $\mathbb{S}^2$ is the curve making a constant bearing angle β with meridians in the orthonormal frame $(\mathbf{e}_\theta, \mathbf{e}_\phi)$. Its differential equation is

$$\frac{d\phi}{d\theta} = \frac{\tan\beta}{\sin\theta}, \qquad \Rightarrow \qquad \phi(\theta) = \phi_0 + \tan\beta\ \ln\tan\Big(\frac{\theta}{2}\Big), \tag{31}$$

where ϕ_0 sets the phase at a reference θ. The seam crossings are the discrete set of points (θ_m, ϕ_m) where γ_+ meets (30), i.e.

$$\phi(\theta_m) \equiv 0,\ \frac{\pi}{2},\ \pi,\ \frac{3\pi}{2}\ (\mathrm{mod}\ 2\pi) \quad \text{or} \quad \theta_m = \frac{\pi}{2}. \tag{32}$$

The induced ordered seam list $\mathcal{E}(\gamma_+)$ is obtained by sorting the θ_m in forward-time order along γ_+ and recording the adjacent-domain transition $(i_m \to i_{m+1})$ at each crossing.

(ii) Chirality connection as α-order Berry connection of the 5D→4D mixing map

Let $U(\theta,\phi)$ denote the (internal) 5D→4D holonomy/basis-mixing map on the electron sheet along forward transport. We expand it in the CP-odd chiral sector as

$$U(\theta,\phi) = \exp(\alpha X_\chi(\theta,\phi) + O(\alpha^2)), \tag{33}$$

where X_χ is an anti-Hermitian generator in the chiral mixing subspace and transforms as

$$(\mathcal{CP})^* X_\chi = -X_\chi. \tag{34}$$

For a transported internal state $|\psi_5\rangle$ on $\mathbb{S}^2_{\rm p}$, define the associated U(1) Berry-type one-form by

$$\omega_\chi := \mathrm{Im}\,\langle\psi_5|\,U^{-1}dU\,|\psi_5\rangle. \tag{35}$$

Using (33), the leading term is

$$\omega_\chi^{(1)} = \mathrm{Im}\,\langle\psi_5|\,dX_\chi\,|\psi_5\rangle, \tag{36}$$

which is CP-odd by (34). The defect entering (21) at order α is the 4D-invisible component

$$\delta\omega_{\rm CP}^{(1)} = (I-\Pi)\omega_\chi^{(1)}. \tag{37}$$

Milestone M1 is: compute $\omega_\chi^{(1)}$ from the explicit holonomy rule $X_\chi(\theta,\phi)$, then compute its seam cocycle induced by $(I-\Pi)$ on the octant cover.

(iii) Bulk–seam computation of chirality: local exactness, seam transitions, and the integer data

Assume (and then verify) that the projected defect is locally exact on each octant:

$$(I-\Pi)\omega_\chi^{(1)}\big|_{\mathcal{D}_i} = d\psi_i^{(1)}. \tag{38}$$

Then for each oriented seam crossing $e=(i\to j)\in\mathcal{E}(\gamma_+)$, the seam jump is

$$\Delta\varphi_{ij}^{(\mathrm{CP},1)} = \psi_j^{(1)}\big|_e - \psi_i^{(1)}\big|_e. \tag{39}$$

The order-α contribution to the invariant is the seam sum

$$\Delta_{\rm CP}^{(1)} = \frac{1}{2\pi}\sum_{(i\to j)\in\mathcal{E}(\gamma_+)} \Delta\varphi_{ij}^{(\mathrm{CP},1)}. \tag{40}$$

Thus, $p\geq 2$ if and only if $\Delta_{\rm CP}^{(1)}=0$.

Octant quantization mechanism. Quantization of the seam jumps arises from the transition functions of the oriented orthonormal frame used to define the chiral generator. Let $(\mathbf{e}_\theta,\mathbf{e}_\phi)$ be the standard oriented frame on each domain. Across a seam, the frame is related by an SO(2) rotation (a gauge transform)

$$(\mathbf{e}_\theta,\mathbf{e}_\phi)_j = R(\Delta\gamma_{ij})\,(\mathbf{e}_\theta,\mathbf{e}_\phi)_i, \qquad R(\Delta\gamma) = \begin{pmatrix}\cos\Delta\gamma & -\sin\Delta\gamma\\ \sin\Delta\gamma & \cos\Delta\gamma\end{pmatrix}. \tag{41}$$

If X_χ is built from an oriented scalar (chirality) measured in that frame, then the seam discontinuity of the local primitive $\psi_i^{(1)}$ is controlled by the frame rotation angle $\Delta\gamma_{ij}$. For the octant cover (30), the natural seam frame rotations are multiples of the octant increment $\pi/4$, hence

$$\Delta\varphi_{ij}^{(\mathrm{CP},1)} = m_{ij}\,\frac{\pi}{4}, \qquad m_{ij}\in\mathbb{Z}, \tag{42}$$

recovering the integer data used in (28) and (29).

(iv) Concrete computable choice: oriented turning of the loxodrome tangent

To make $\omega_\chi^{(1)}$ explicitly computable from the seam loop, choose X_χ to be proportional to the oriented turning angle of the loxodrome tangent relative to the domain frame. Let T be the unit tangent to the loxodrome and write in the orthonormal frame

$$T = \cos\beta\, \mathbf{e}_\theta + \sin\beta\, \mathbf{e}_\phi, \tag{43}$$

with constant bearing angle β. Define a chiral phase χ by the frame-angle of T:

$$\chi := \arg(T) = \beta \pmod{2\pi} \text{ on each domain}, \tag{44}$$

and define the chiral generator

$$X_\chi := i\,\chi\, P_\chi, \tag{45}$$

where P_χ is the projector onto the CP-odd internal mixing channel selected by $(I - \Pi)$. Then $\omega_\chi^{(1)} = d\chi$ on each domain, so (38) holds with $\psi_i^{(1)} = \chi|_{\mathcal{D}_i}$. The entire holonomy is therefore carried by seam jumps: when γ_+ crosses a seam, the local frame rotates by $\Delta\gamma_{ij}$ and the represented tangent-angle χ shifts by $\Delta\gamma_{ij}$, giving

$$\Delta\varphi_{ij}^{(\mathrm{CP},1)} = \Delta\gamma_{ij}. \tag{46}$$

Thus Milestone M1 reduces to a purely geometric calculation: compute the ordered seam-crossing list $\mathcal{E}(\gamma_+)$, compute the frame-rotation angles $\Delta\gamma_{ij}$ induced by the seam transitions on the octant cover, and sum them in (40). If the sum vanishes by antipodal pairing, then $p \geq 2$; if not, $p = 1$ and $\tau_{\mathrm{CP}} = \sum m_{ij}$ is fixed.

9.5 Obstruction classes from domain stitching

On a single domain $\mathcal{D}_i$, suppose the leading defect is exact:

$$(I - \Pi)\omega_\chi^{(1)}\big|_{\mathcal{D}_i} = d\psi_i. \tag{47}$$

Then $\oint_{\partial\mathcal{D}_i} d\psi_i = 0$ and the only surviving contributions to Δ_{CP} come from *stitching mismatches* $\psi_i - \psi_j$ across boundaries. Those mismatches are precisely the phase jumps $\Delta\varphi_i^{(\mathrm{CP})}$ in (16). The obstruction index τ_{CP} in (17) is then the cohomology class of the boundary jump 1-cocycle on the domain adjacency graph.

In the antipodal $N = 8$ taxonomy, exact pairing implies $\tau_{\mathrm{CP}} = 0$. A nonzero τ_{CP} requires a packing obstruction (e.g., a chiral defect line or unpaired twist) that prevents a global choice of $\{\psi_i\}$ making all boundary mismatches cancel.

10 Metrology: frequency shift in QMU

Define the electron action scale

$$h_e := m_{\mathrm{e}}\, {\lambda_C}^2\, F_q. \tag{48}$$

Then $\Delta f = \Delta U / h_e$ gives

$$\Delta f = -\frac{{e_{\mathrm{emax}}}^2\, \lambda_C}{h_e}\, \Delta_{\mathrm{CP}}\, (\hat{\mathbf{s}} \cdot \nabla\Phi_Q). \tag{49}$$

In polar-molecule and molecular-ion EDM platforms, internal structure produces a large, effectively fixed axis $\hat{\mathbf{n}}$ and a correspondingly large internal driver along that axis; see representative platforms and progression of limits in Hudson et al. [2002], Baron et al. [2014], Andreev et al. [2018], Roussy et al. [2023] and the broader perspective in Safronova et al. [2018], Chupp et al. [2019]. Define the internal reciprocal-capacitance gradient component

$$\mathcal{G}_{\text{eff}} := \hat{\mathbf{n}} \cdot \nabla \Phi_Q, \tag{50}$$

so that for spin prepared parallel/antiparallel to $\hat{\mathbf{n}}$,

$$\Delta f_{\uparrow\downarrow} = 2\, \frac{{e_{\text{emax}}}^2\, \lambda_C}{h_e}\, |\Delta_{\text{CP}}|\, |\mathcal{G}_{\text{eff}}|. \tag{51}$$

11 Predictions, experimental discriminators, and next derivation milestones

11.1 Predictions in the QMU/Aether-unit framing

The present formulation yields the following predictions without importing point-parameter EDM assumptions.

(P1) Geometric observable, not point parameter. The fundamental EDM observable is the square-charge first moment $\mathbf{D}_{e^2}$ in (4), not a scalar coefficient attached to a point.

(P2) Correct driver is $\nabla\Phi_Q$, not a legacy field primitive. The energy shift is governed by $\Delta U = -\mathbf{D}_{e^2} \cdot \nabla \Phi_Q$ in (5), with $\Phi_Q = 1/C$. Thus experimental "sensitivity" must be analyzed in terms of the internal reciprocal-capacitance gradient $\mathcal{G}_{\text{eff}}$ in (50).

(P3) Structural neutrality unless obstruction. In the antipodally paired domain taxonomy, intrinsic CP-odd holonomy cancels unless a genuine packing obstruction exists. Equivalently, $\Delta_{\text{CP}} = 0$ unless $\tau_{\text{CP}} \neq 0$ in (17).

(P4) If nonzero, the EDM is quantized and α-suppressed. When an obstruction class is admissible, Δ_{CP} takes a discrete spectrum $\Delta_{\text{CP}} = \alpha^p \tau_{\text{CP}}/8$ with integer τ_{CP}. Continuous "tuning" is replaced by discrete microstate classes.

(P5) Apparent probabilistic behavior is an ensemble statement. Observed bounds constrain the admissible microstate set $\mathcal{S}$ and/or the packing weights $w(s)$ in (14); randomness is not primitive, but emergent from preparation-dependent weighting.

11.2 Experimental discriminators

The following experiment classes test the specifically QMU/geometry claims above.

(E1) Driver collapse test across platforms. Compare multiple EDM platforms by plotting extracted shifts against a modeled $\mathcal{G}_{\text{eff}} = \hat{\mathbf{n}} \cdot \nabla \Phi_Q$ rather than against a legacy "effective field" proxy. The QMU hypothesis predicts tighter cross-platform consistency when the driver is expressed as $\nabla\Phi_Q$.

(E2) Handedness (enantiomer) discriminator for ensemble bias. If a platform can be realized in opposite macroscopic handedness environments, test whether the inferred $\langle \Delta_{\mathrm{CP}} \rangle$ tracks a change in microstate weights $w(s)$ rather than appearing as a fixed intrinsic constant. This separates intrinsic obstruction ($\tau_{\mathrm{CP}} \neq 0$) from preparation bias.

(E3) State-preparation weighting tests. Vary preparation protocols that plausibly reweight admissible packing microstates (rotational state selection, pulse schedules, trap geometry, temperature/rotational cooling). The ensemble model predicts controlled changes in $\langle \Delta_{\mathrm{CP}} \rangle$ even when legacy narratives expect invariance.

(E4) Cross-sector consistency web. Because electrostatic polarity is a two-sheet Aether dipole while magnetic dipole structure is intrinsic to each spin position, compare the pattern of constraints inferred from electron-sensitive platforms to those inferred from proton-sector (baryonic) EDM searches, as discussed in the EDM overview literature Chupp et al. [2019], Safronova et al. [2018].

11.3 Next derivation milestones (to convert structure to numbers)

Milestone M1 (fix the leading order p). Compute $\omega_\chi^{(1)}$ in (18) from the explicit 5D→4D holonomy map on the Aether unit and evaluate whether $\oint (I - \Pi)\omega_\chi^{(1)} = 0$. If it vanishes by symmetry/exactness, then $p \geq 2$; otherwise $p = 1$. A computable octant-seam reduction and explicit $\omega_\chi^{(1)}$ framework are given in §9.4. Now that the Canonical Octant Labeling is fixed (Section 9.4, M2.3), the next step is to execute the *numerical* seam summation for the electron by enumerating the ordered loxodromic seam-crossing list $\mathcal{E}(\gamma_+)$, assigning each crossing its adjacent-octant transition $(i \to j)$, and summing the corresponding integers m_{ij} defined by $\Delta\varphi_{ij}^{(\mathrm{CP},1)} = m_{ij}(\pi/4)$. This produces $\tau_{\mathrm{CP}} = \sum_{(i\to j)\in\mathcal{E}(\gamma_+)} m_{ij}$ and therefore the leading invariant $\Delta_{\mathrm{CP}} = \alpha^p \tau_{\mathrm{CP}}/8$. If Milestone M1 yields $p = 1$ and the explicit seam loop evaluation gives the minimal nontrivial obstruction $\tau_{\mathrm{CP}} = 1$, then the theory makes a parameter-free magnitude prediction in native QMU units, $|\mathbf{D}_{e^2}| = {e_{\mathrm{emax}}}^2\, \lambda_C\, (\alpha/8)$, with the sign and spin alignment fixed by the seam orientation and $\hat{\mathbf{s}}$.

Milestone M2 (classify admissible obstruction classes). Determine whether the electron packing admits $\tau_{\mathrm{CP}} \neq 0$ (a nontrivial boundary-jump cocycle) or whether two-sheet pairing forces $\tau_{\mathrm{CP}} \equiv 0$. This decides "EDM strictly zero" versus "EDM quantized."

Milestone M3 (derive $\mathcal{G}_{\mathrm{eff}}$ in QMU for candidate platforms). For specific molecular/ionic geometries, compute or bound $\hat{\mathbf{n}} \cdot \nabla\Phi_Q$ from their packing geometry and show how reported sensitivity re-expresses in QMU driver language.

A Legacy reporting bridge (appendix only)

Legacy literature reports an "electron EDM" in units of (charge) · (length), e.g. $e \cdot \mathrm{cm}$. In QMU the primitive observable is $\mathbf{D}_{e^2}$ with unit ${e_{\mathrm{emax}}}^2 \cdot \lambda_C$. A square-charge-consistent bridge is obtained by comparing *squared* energy shifts. If legacy reporting quotes a bound $|d_e| < d_{\mathrm{max}}$ in linear-charge units, then the corresponding square-charge dipole bound can be written as

$$|\mathbf{D}_{e^2}|^2 < e^2\, d_{\mathrm{max}}^2 \qquad \text{(bridge identity)}. \tag{52}$$

Using the electron charge-basis map from the CCF definition Thomson [2025a],

$$e^2 = 8\pi\alpha\, {e_{\text{emax}}}^2, \tag{53}$$

so (52) becomes

$$|\mathbf{D}_{e^2}|^2 < 8\pi\alpha\, {e_{\text{emax}}}^2\, d_{\text{max}}^2. \tag{54}$$

Combining with (12) gives an experimental constraint on the CP-holonomy amplitude:

$$\Delta_{\text{CP}}^2 < \frac{8\pi\alpha\, d_{\text{max}}^2}{{e_{\text{emax}}}^2\, {\lambda_C}^2}. \tag{55}$$

For SI-to-QMU conversion tables and constants, use the QMU reference tables Thomson [2025b].

B Null bound citation

State-of-the-art experiments report strong null bounds on the electron EDM; see, e.g., the trapped-molecular-ion result Roussy et al. [2023] and the ACME beam benchmarks Andreev et al. [2018], Baron et al. [2014].

Acknowledgments

The Quantum AetherDynamics Institute (QADI) is a private 501(c)(3) research institute developing the Aether Physics Model (APM) and Quantum Measurement Units (QMU) Quantum AetherDynamics Institute (QADI) [2025]. Publications and data are archived with DOIs in the AetherPhysics Zenodo community: zenodo.org/communities/aetherphysics.

References

V. Andreev et al. Improved limit on the electric dipole moment of the electron. *Nature*, 562:355–360, 2018. doi: 10.1038/s41586-018-0599-8. URL https://doi.org/10.1038/s41586-018-0599-8.

J. Baron et al. Order of magnitude smaller limit on the electric dipole moment of the electron. *Science*, 343(6168):269–272, 2014. doi: 10.1126/science.1248213. URL https://doi.org/10.1126/science.1248213.

T. E. Chupp, M. J. Ramsey-Musolf, and J. Suhonen. Electric dipole moments of atoms, molecules, nuclei, and particles. *Reviews of Modern Physics*, 91:015001, 2019. doi: 10.1103/RevModPhys.91.015001. URL https://doi.org/10.1103/RevModPhys.91.015001.

J. J. Hudson, B. E. Sauer, M. R. Tarbutt, and E. A. Hinds. Measurement of the electron electric dipole moment using ybf molecules. *Physical Review Letters*, 89:023003, 2002. doi: 10.1103/PhysRevLett.89.023003. URL https://doi.org/10.1103/PhysRevLett.89.023003.

Maxim Pospelov and Adam Ritz. Electric dipole moments as probes of new physics. *Annals of Physics*, 318(1):119–169, 2005. doi: 10.1016/j.aop.2005.04.002. URL https://doi.org/10.1016/j.aop.2005.04.002.

Quantum AetherDynamics Institute (QADI). Quantum aetherdynamics institute (qadi): Community doi overview and citation guide, 2025. URL https://doi.org/10.5281/zenodo.17479314.

T. S. Roussy et al. A new bound on the electron's electric dipole moment. *Science*, 2023. doi: 10.1126/science.adg4084. URL https://doi.org/10.1126/science.adg4084.

M. S. Safronova, D. Budker, D. DeMille, D. F. J. Kimball, A. Derevianko, and C. W. Clark. Search for new physics with atoms and molecules. *Reviews of Modern Physics*, 90:025008, 2018. doi: 10.1103/RevModPhys.90.025008. URL https://doi.org/10.1103/RevModPhys.90.025008.

David Thomson. The charge conversion factor in the aether physics model: From singular to distributed charge, with rules, exceptions, and benchmarks, 2025a. URL https://doi.org/10.5281/zenodo.17451188.

David Thomson. Reference tables for quantum measurement unit (qmu) conversions: Cgs and mks systems, 2025b. URL https://doi.org/10.5281/zenodo.17683574.